

Strain-induced pseudo-magnetic field for novel graphene electronics

Tony Low* and F. Guinea†

*Network for Computational Nanoelectronics, Hall for Discovery Learning Research
Purdue University, West Lafayette, IN47907-1791 Indiana, US

†Instituto de Ciencia de Materiales de Madrid, CSIC,
Sor Juana Inés de la Cruz 3, E28049 Madrid, Spain

Particular strain geometry in graphene could lead to a uniform pseudo-magnetic field of order 10T and might open up interesting applications in graphene nano-electronics. Through quantum transport calculations of realistic strained graphene flakes of sizes of 100nm, we examine possible means of exploiting this effect for practical electronics and valleytronics devices. First, we found that elastic backscattering at rough edges leads to the formation of well defined transport gaps of order 100meV under moderate maximum strain of 10%. Second, the application of a real magnetic field induced a separation, in space and energy, of the states arising from different valleys, leading to a way of inducing bulk valley polarization which is insensitive to short range scattering.

PACS numbers:

Introduction. The isolation of single layer graphene, and the possibility of controlling the electronic carrier density[1-3] has led to a large research effort, because of the novel fundamental features exhibited by graphene and also its possible applications[4, 5]. Graphene is a two dimensional membrane whose electronic properties can be controlled by applying a gate voltage. It can be shown that the elastic deformations of the membrane modify the electronic properties, as they play the role of an effective gauge field[4, 6, 7], opening a new way of tailoring the electronic properties. Strains of at least 10% can be induced in graphene without damaging appreciably its structure[8]. Suspended graphene samples show long range deformations on scales of hundreds of nanometers[9-11], and strains can be induced in graphene samples by different techniques[12-14].

Strains can be expected to arise naturally in suspended samples[15]. It has been shown that a uniformly varying strain leads to a gauge potential which generates an effective constant magnetic field[16, 17] (time reversal symmetry implies that the field has opposite signs in the two valleys). The field due to strains can interfere in many ways with real magnetic fields[18]. Other schemes to use strains[19] to tune the electronic properties have also been proposed. Strains can possibly be manipulated efficiently in samples with good adhesion to the substrate, such as graphene layers grown epitaxially on SiC. Hence, the proposed effects in this paper could be tested experimentally.

As discussed in[17], an effective constant magnetic field arises from strains varying at a constant rate. We discuss here the electronic properties of graphene flakes under the combined effect of strains, magnetic fields and disorder. We use the setup proposed in[17] as a way of inducing an almost constant effective magnetic field. The model

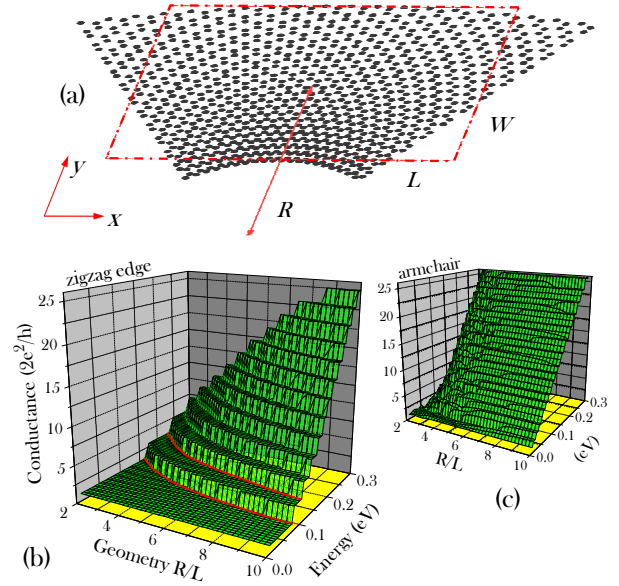


FIG. 1: (a) Sketch of an example strain geometry with a maximum strain of 50%. Note that the actual size of the flake used in this paper is much larger, i.e. $L = W = 100\text{nm}$, and with much smaller maximum strain (see text). Conductance as a function of Fermi energy and strained geometry characterized by R/W for (b) zigzag and (c) armchair edge ribbons, in the absence of real magnetic field and edge disorder. The dimension of the graphene flake is $L = W = 100\text{nm}$.

and method of calculation are discussed in the next section. Then, we present the main results. The last section discusses the main conclusions of our work.

The model. A strain distribution, u_{ij} , leads to the effective gauge field[6, 7, 16],

$$\tilde{\mathbf{A}} = \frac{c\beta}{a_0} \begin{pmatrix} u_{xx} - u_{yy} \\ -2u_{xy} \end{pmatrix} \quad (1)$$

where $\beta \approx \partial \log(t) / \partial \log(a)|_{a=a_0} \approx 2-3$, $a_0 \approx 1.4 \text{ \AA}$ is the lattice constant, $t \approx 3\text{eV}$ is the nearest neighbor coupling

*Electronic address: tonyaslow@gmail.com

†Electronic address: paco.guinea@icmm.csic.es

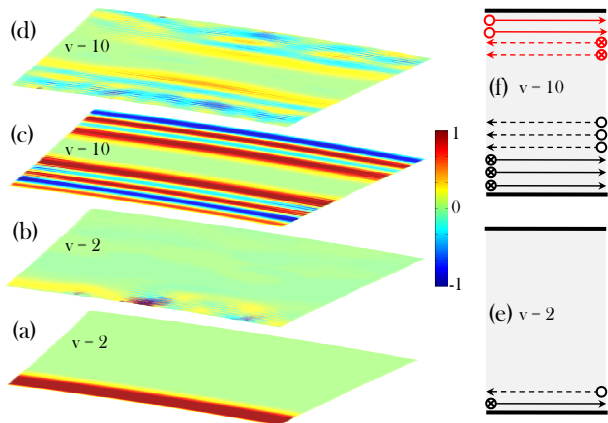


FIG. 2: The non-equilibrium current density $\text{sign}(j_x) \times |j(x, y)|$ intensity plot for a $100 \times 100 \text{nm}$ graphene flake under a strain of $R/W = 5$ (equivalent to $B_s \approx 9\text{T}$) at ϵ_F corresponding to filling factor $\nu = 2$ (a) without edge disorder and (b) with edge disorder. Similar plots in (c-d) but for filling factor $\nu = 10$ instead. The color scale indicated is normalized with respect to $\max(|j(x, y)|)$. Red/blue color indicates current flowing to the right/left of the device. (e) and (f) illustrates the counter-propagating edge states at $\nu = 2$ and $\nu = 10$ respectively.

energy and c is a dimensionless constant of order unity. The main axes of the graphene lattice in Eq. 1 has been chosen so that the x axis coincides with a zigzag direction. We assume that the distortions have been induced by bending a flake in the way discussed in [17]

$$(u_x, u_y) = \left(\frac{xy}{R}, -\frac{x^2}{2R} \right) \quad (2)$$

where R is the bending radius of the deformation applied to the flake, see Fig. 1a. This would translate to a pseudomagnetic field strength of $B_s = c\beta/a_0R \equiv \Omega W/R$, where Ω is to be determined numerically.

To compute the transport properties, we adopt a nearest neighbor hopping between π orbitals in the honeycomb lattice [20],

$$\mathcal{H} = \sum_{ij} \left[t_0 \left(1 + \beta \frac{\delta d_{ij}}{a_0} \right) \right] \exp \left(\frac{e}{\hbar} \int_i^j \mathbf{A} \cdot d\mathbf{l} \right) a_i^\dagger a_j \quad (3)$$

where δd_{ij} is the change in bond length, and \mathbf{A} is the real gauge field, whose effect is incorporated as a Peierls phase. We assumed $t_0 = 3\text{eV}$ and $\beta = 2$. Semi-infinite leads are assumed for the left and right boundaries. The numerical methods that we had employed to compute the transmission function T is the recursive green function[21–23] and the renormalization method[24]. The Landauer formula then gives us the zero temperature conductance i.e. $2e^2/h \times T$ [25]. Details of the implementation had already been documented elsewhere[26, 27].

We consider square graphene flakes with dimensions $W = L = 100\text{nm}$ where the origin for the deformation

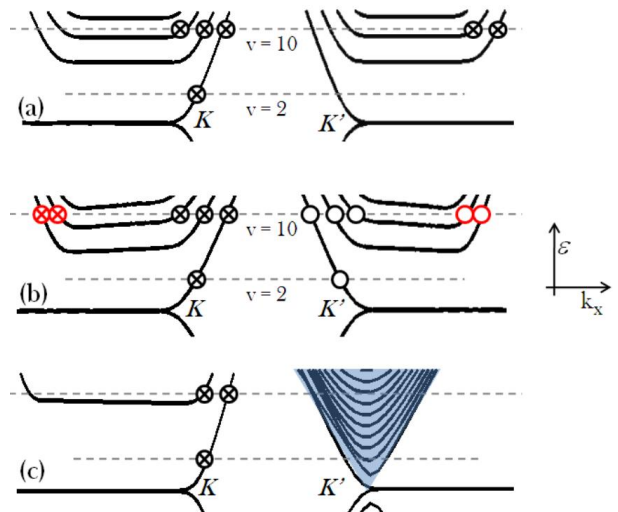


FIG. 3: Plot of typical energy dispersion as a function of momentum along the transport direction for the case of (a) real magnetic field $B = 9\text{T}$, (b) pseudomagnetic field $B_s = 9\text{T}$ and (c) $B_s = B = 9\text{T}$. The symbols \otimes and \circ denotes the sign of the field, while red/black color denotes whether the chiral edge states are propagating along the top/bottom edge. The highlighted bulk states in (c) are non-chiral i.e. it feels an effective zero magnetic field.

in Eq. 2 is the center of the flake. The maximum strain exerted would then be along the two edges, which is given by $\max(u_{xx}) \approx W/2R$.

Results. We show in Fig.1b and c the computed conductance as a function of R/W and energy for zigzag and armchair edge ribbons respectively. Clean quantum Hall plateaus are observed for the zigzag ribbons with filling factors given by $\nu = 2, 6, 10 \dots = 4n + 2$, exactly mimicking the conventional quantum Hall case. Knowing that the first excited Landau energy $\epsilon_1 = \nu_F \sqrt{2\hbar B e}$ in the conventional quantum Hall case, we can estimate numerically the effective magnetic field induced by a deformation characterized by the ratio W/R as for $B_s = \Omega W/R$ with $\Omega \approx 45\text{T}$, in good agreement with the estimates in [16, 17].

The effects on the electronic states of a uniaxial strain, $u_{xx}(x)$, like the one studied here, depend strongly on the orientation of the lattice with respect to the direction of the strains. When the y axis coincides with an armchair direction, a gauge field along the x direction is generated, $A_x(y)$, and an effective magnetic field ensues (see for example simpler case of a one-dimensional ripple [28]). On the other hand, when the y axis is along a zigzag direction, the gauge field due to the uniaxial strain can be written as $A_y(y)$. This gauge field does not induce an effective magnetic field, and leaves the electronic spectrum unchanged. The results in Fig. 1 are in agreement with this analysis. Hereafter, we shall only consider zigzag ribbons with strain geometry $R/W = 5$, which yields $B_s \approx 9\text{T}$.

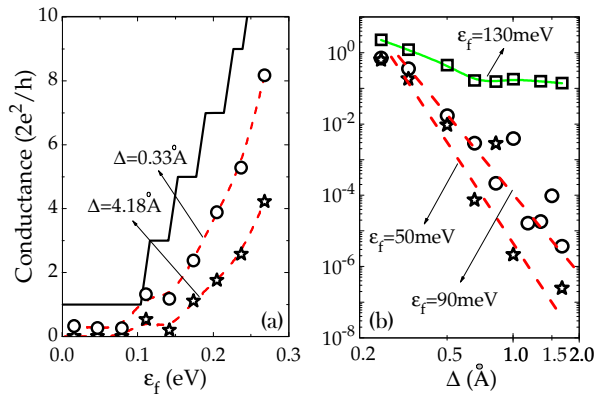


FIG. 4: Zero temperature conductance as a function of (a) Fermi energy ϵ_f and (b) edge disorder Δ , for different values of Δ and ϵ_f respectively. Zigzag ribbon is assumed and the strain geometry employed corresponds to $W/R = 5$. The solid line for (a) is for the case of zero disorder.

Unlike the case in the Quantum Hall effect, the edge states are not protected by time reversal symmetry, and they can be affected by elastic backscattering. Fig. 2 a and c plots the non-equilibrium current density at Fermi energy corresponding to $\nu = 2$ and $\nu = 10$. For $\nu = 2$, strains induce two edge modes, which propagate in opposite directions. Time reversal symmetry implies that these two modes are localized at the same edge, in agreement with the numerical results. In general, the compressive strained edge would acquire two more modes than the other edge. The zigzag boundary condition used here do not mix the K and K' valleys, leading to a clear distinction of the edge modes.

The zigzag boundary condition (where a given edge can be characterized by a majority sublattice) is generic for graphene edges[29], except the armchair one. The edge modes induced by strains have a characteristic width of order of the effective magnetic length associated to the strain field, $\ell_s \approx \sqrt{(a_0 L)/(\beta \bar{u})}$, where L is a typical length which describes the variation of the strain, and \bar{u} is the average strain. Typically $\ell_s \gg a_0$, and the continuum zigzag boundary conditions discussed in[29] describe well the numerical results.

The physical origin of the edge currents is explained in Fig. 3a and b, which plots the corresponding energy dispersion along the transport direction for the case with a real and pseudomagnetic field respectively. For the latter, one makes the observation that for a given current direction, the edge states on the two edges are valley polarized i.e. quantum valley Hall effect. This effect is analogous to the quantum spin Hall effect[30]. In both cases, the net pseudo-gauge field of the system is zero, but finite and opposite for each spin/valley. However, in this case, short-range scattering would couples the valleys. Since the counter propagating edge states residing along a particular edge belongs to different valleys, intervalley processes lead to backscattering. In the presence of edge disorder, substantial backscattering can occurs

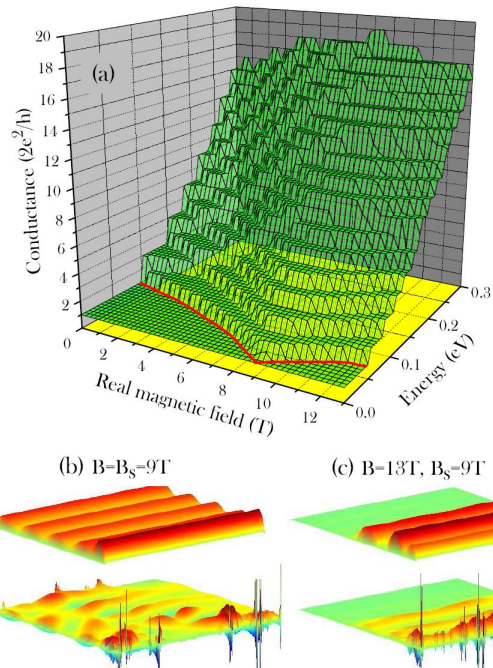


FIG. 5: (a) shows the conductance as a function of real magnetic field and Fermi energy, calculated for non-disordered zigzag ribbon with a strain geometry corresponding to $W/R = 5$, which is equivalent to $B_s \approx 9T$. (b) plots the current density at $\epsilon_f = 0.1eV$ for the condition $B = B_s = 9T$, for perfect edge (top) and disorder edges (bottom). Similar plots for (c), except now for the condition of $B = 13T$ and $B_s = 9T$. The color scheme employed is the same as Fig. 2.

and Anderson localization spots can be observed (see Fig. 2b). A more quantitative evaluation of the impact of edge roughness follows.

The edge roughness is generated using a procedure outlined in[27]. The roughness morphologies generated were assumed to have an autocorrelation length of 2nm and a root-mean-square roughness Δ , where $0.2\text{\AA} \leq \Delta \leq 5\text{\AA}$ is used as the disorder parameter in this work. Fig. 4a plots the energy resolved conductance for various values of Δ . Disorder at the edges opens a transport gap ϵ_g , and the flake shows insulating behavior near the neutrality point. When the disorder increases, ϵ_g saturates to a value of the order of two times the energy of the first effective Landau level, modulated by the strain via $\epsilon_g \propto \sqrt{W/R}$. In the nanoribbon counterpart, it was found to behave as $\epsilon_g \propto 1/W$ [31]. The pseudomagnetic length is given by $\ell_s \propto \sqrt{R/W}$, which approximates the spatial extent of the ground state Landau wavefunction from the edges, can be of order of $10nm$ at moderate strain of $W/R = 5$. The estimates in the Supplementary Information in[16] suggest a localization length for the edge modes, due to intervalley scattering of order $\xi \approx (\ell_s/a_0)^2 n_v^{-1}$, where n_v is the one dimensional density of vacancies at the edges. For a rough edge on atomic scales, $n_v \sim 10nm^{-1}$, so that $\xi \sim W$, and localization can be expected for the strains

and dimensions used here.

Next, we examine the interplay between real and pseudomagnetic field. Their combined contribution is such that the valleys feel an effective field of $\tilde{\mathbf{A}} \pm \mathbf{A}$. Fig. 5a shows the conductance for varying B field but at $B_s \approx 9T$. Splitting of the conductance plateaus steps from $4n + 2$ into $2n + 2$ can be observed, with decreasing plateau width for $n = 0$. An interesting situation arises when $B = B_s$, where Fig. 3c illustrates the corresponding energy dispersion. The cancellation of the field for \mathbf{K}' valley leads to a recovery of the bulk band dispersion. Hence, the conductance goes as $\approx c\epsilon_f + 2$, where the latter contribution comes from the \mathbf{K} valley. This provides a feasible avenue for producing valley polarized electrons, since it does not depend on good quality at the edges like in previous proposal[32]. We note that in general, these bulk states are not protected by time reversal symmetry. Fig. 5b plots the current density at the condition $B = B_s = 9T$, with/without edge disorder. Their respective conductances (in $2e^2/h$) are 5 and 3.3 respectively. At larger magnetic field, say $B = 13T > B_s = 9T$, edge states emerge and now the conductance remains at 3 with/without edge disorder. Fig. 5c shows the respective current density plots.

Conclusions. We have analyzed in detail the electronic properties of graphene flakes under the combined effect of strains, magnetic fields and disorder. We analyze numerically the electronic spectrum of flakes of realistic sizes,

$\sim 100\text{nm}$ with strain distributions that generate a constant effective magnetic field. Strains induce gaps in the bulk spectrum and propagating modes along the edges. The edge modes are valley polarized, and strongly suppressed at armchair edges, where the boundary condition strongly mixes the different valleys [33]. The two lowest edge modes are localized at the same edge. In general, the number of edge modes differs by two between the two edges.

Possible device applications are addressed. First, disorder leads to backscattering, which is more significant for the lowest edge (see Fig. 4b). We find a clear transport gap near the Dirac energy, leading to new ways of developing graphene transistors. Second, the interference between real magnetic fields and the gauge field due to strains lead to the separation in space and in energy of the states from the two valleys. Because of this separation, the valley polarization achieved in this way is not much affected by intervalley scattering, opening a way of obtaining valley polarized bulk currents.

Acknowledgements. We are grateful to A. K. Geim, M. I. Katsnelson, K. S. Novoselov and M. Lundstrom for useful discussions and Network of Computational Nanoelectronics for computational support. F. G. acknowledges funding from MICINN (Spain), through grants FIS2008-00124 and CONSOLIDER CSD2007-00010. T. L. acknowledges funding from the Institute for Nanoelectronics Discovery and Exploration.

-
- [1] K. S. Novoselov, A. K. Geim, S. V. Morozov, D. Jiang, Y. Zhang, S. V. Dubonos, I. V. Grigorieva, and A. A. Firsov, *Science* **306**, 666 (2004).
 - [2] K. S. Novoselov, D. Jiang, F. Schedin, T. J. Booth, V. V. Khotkevich, S. V. Morozov, and A. K. Geim, *Proc. Natl. Acad. Sci. U.S.A.* **102**, 10451 (2005).
 - [3] K. S. Novoselov, A. K. Geim, S. V. Morozov, D. Jiang, M. I. Katsnelson, I. V. Grigorieva, S. V. Dubonos, and A. A. Firsov, *Nature* **438**, 197 (2005).
 - [4] A. H. Castro Neto, F. Guinea, N. M. R. Peres, K. S. Novoselov, and A. K. Geim, *Rev. Mod. Phys.* **81**, 109 (2009).
 - [5] A. K. Geim, *Science* **324**, 1530 (2009).
 - [6] H. Suzuura and T. Ando, *Phys. Rev. B* **65**, 235412 (2002).
 - [7] J. L. Mañes, *Phys. Rev. B* **76**, 045430 (2007).
 - [8] C. Lee, X. Wei, J. W. Kysar, and J. Hone, *Science* **321**, 385 (2008).
 - [9] J. S. Bunch, A. M. van der Zande, S. S. Verbridge, I. W. Frank, D. M. Tanenbaum, J. M. Parpia, H. G. Craighead, and P. L. McEuen, *Science* **315**, 5811 (2007).
 - [10] T. J. Booth, P. Blake, R. R. Nair, D. Jiang, E. W. Hill, U. Bangert, A. Bleloch, M. Gass, K. S. Novoselov, M. I. Katsnelson, and A. K. Geim, *Nano Lett.* **8**, 2442 (2008).
 - [11] W. Bao, F. Miao, Z. Chen, H. Zhang, W. Jang, C. Dames, and C. N. Lau, *Nature Nanotechnology* **4**, 562 (2009).
 - [12] T. M. Mohiuddin, A. Lombardo, R. R. Nair, A. Bonetti, G. Savini, R. Jalil, N. Bonini, D. M. Basko, C. Galotisi, N. Marzari, et al., *Phys. Rev. B* **79**, 205433 (2009).
 - [13] M. Huang, H. Yan, C. Chen, D. Song, T. F. Heinz, and J. Hone, *Proc. Nat. Acad. Sci.* **106**, 7504 (2009).
 - [14] J. E. Proctor, E. Gregoryanz, K. S. Novoselov, M. Lotya, J. N. Coleman, and M. P. Halsall, *Phys. Rev. B* **80**, 073408 (2009).
 - [15] M. M. Fogler, F. Guinea, and M. I. Katsnelson, *Phys. Rev. Lett.* **101**, 226804 (2008).
 - [16] F. Guinea, M. I. Katsnelson, and A. K. Geim, *Nature Physics* **6**, 30 (2010).
 - [17] F. Guinea, A. K. Geim, M. I. Katsnelson, and K. S. Novoselov, *Physical Review B* **81**, 035408 (2010).
 - [18] E. Prada, P. San-Jose, G. León, M. M. Fogler, and F. Guinea (2009), arXiv:0906.5267.
 - [19] V. M. Pereira and A. H. Castro Neto, *Phys. Rev. Lett.* **103**, 046801 (2009).
 - [20] P. R. Wallace, *Phys. Rev.* **71**, 622 (1947).
 - [21] S. Datta, *Electronic Transport in Mesoscopic System*, Cambridge University Press (1997).
 - [22] S. Nonoyama and A. Oguri, *Phys. Rev. B* **57**, 8797 (1998).
 - [23] M. P. Anantram, M. S. Lundstrom, and D. E. Nikonov, *Proc. IEEE* **96**, 1511 (2008).
 - [24] G. Grosso, S. Moroni, and G. P. Parravicini, *Phys. Rev. B* **40**, 328 (1989).
 - [25] R. Landauer, *Philos. Mag.* **21**, 863 (1970).
 - [26] T. Low and J. Appenzeller, *Phys. Rev. B* **80**, 155406 (2009).
 - [27] T. Low, *Phys. Rev. B* **80**, 205423 (2009).
 - [28] F. Guinea, M. I. Katsnelson, and M. A. H. Vozmediano,

- Phys. Rev. B **77**, 075422 (2008).
- [29] A. R. Akhmerov and C. W. J. Beenakker, Phys. Rev. B **77**, 085423 (2008).
- [30] C. L. Kane and E. J. Mele, Phys. Rev. Lett. **95**, 226801 (2005).
- [31] E. R. Mucciolo, A. H. C. Neto, and C. H. Lewenkopf, Phys. Rev. B **79**, 075407 (2009).
- [32] A. Rycerz, J. Tworzydło, and C. W. J. Beenakker, Nat. Phys. **3**, 172 (2007).
- [33] L. Brey and H. A. Fertig, Phys. Rev. B **73**, 235411 (2006).